

# Clenshaw Graph Neural Networks

Yuhe Guo

Renmin University of China  
Beijing, China  
guoyuhe@ruc.edu.cn

Zhewei Wei

Renmin University of China  
Beijing, China  
zhewei@ruc.edu.cn

## ABSTRACT

Graph Convolutional Networks (GCNs), which use a message-passing paradigm with stacked convolution layers, are foundational methods for learning graph representations. Recent GCN models use various residual connection techniques to alleviate the model degradation problem such as over-smoothing and gradient vanishing. Existing residual connection techniques, however, fail to make extensive use of underlying graph structure as in the graph spectral domain, which is critical for obtaining satisfactory results on heterophilic graphs.

In this paper, we introduce ClenshawGCN, a GNN model that employs the Clenshaw Summation Algorithm to enhance the expressiveness of the GCN model. ClenshawGCN equips the standard GCN model with two straightforward residual modules: the *adaptive initial residual connection* and the *negative second-order residual connection*. We show that by adding these two residual modules, ClenshawGCN implicitly simulates a polynomial filter under the Chebyshev basis, giving it at least as much expressive power as polynomial spectral GNNs. In addition, we conduct comprehensive experiments to demonstrate the superiority of our model over spatial and spectral GNN models.

## KEYWORDS

Graph Neural Networks, Residual Connection, Graph Polynomial Filter

### ACM Reference Format:

Yuhe Guo and Zhewei Wei. 2023. Clenshaw Graph Neural Networks. In *Proceedings of ACM Conference (Conference'17)*. ACM, New York, NY, USA, 10 pages. <https://doi.org/XXXXXXX.XXXXXXX>

## 1 INTRODUCTION

The past few years have witnessed the rise of machine learning on graphs, which considers relations (edges) between elements (nodes) such as interactions among molecules [10, 32], friendship or hostility between users [11, 41], and implicit syntactic or semantic structure in natural language [33, 40].

GCN [18] proposed a message-passing paradigm for Graph Neural Networks that exploits the underlying graph topology by propagating node features iteratively along the edges. Along with the

message-passing steps, each node receives information from growingly expanding neighborhoods. Such a *propagation* entangled with non-linear *transformation* forms a *graph convolution layer* in GCN.

Following ResNet [12], various GNN models use different residual connection techniques to overcome the problem of *model degradation*. As shown in Figure 1, we broadly classify the graph residual connections into three types:

- **Raw Residual Connections** are directly transplanted to GCNs in early attempts [18], but they lose effectiveness when models come deeper [6, 42]. The reason behind this was gradually clarified with the discussion of *over-smoothing* [22, 31].
- **Initial Residual Connections** [6, 19] are intuited by *personalized pagerank*, following the perspective of viewing GCNs with raw residues as *lazy random walk* [38, 42], which converges to the *stationary vector*. Equipped with initial residues, the final representation implicitly leverages features of all fused levels. However, despite its ability to eliminate over-smoothing, models with initial residual connections in fact employ the *homophily assumption* [26], that is, the assumption that connected nodes tend to share similar features and labels, which might be unsuitable for heterophilic graphs [29, 47]. Some variants are also explored [24, 45], but they still fall into the scope of homophily.
- There are also **Dense Residual Connections**, which believe that, by exhibiting feature maps after different times of convolutions and combining them selectively, it is helpful for making extensive use of multi-scale information [1, 42]. The connection pattern in DenseNet [16] is also exploited in [21], where they connect each layer to all former layers, incurs unaffordable space consumption.

*Residual Connections and Polynomial Filters*. On the other hand, the idea of making extensive use of multi-scale representations is closely related to *Spectral Graph Neural Networks*, which motivates us to inject the characteristics of spectral GNNs into our model by residual connections. Spectral GNNs gain their power from utilizing atomic *structural components* decomposed from the underlying graph. Spectral GNNs project features onto these components, and modulate the importance of the components by a *filter*. When this filter is a  $K$ -order *polynomial* function on the graph's Laplacian spectrum, explicit decompositions of matrices are avoided, replaced by additions and subtractions of localized propagation results within different neighborhood radii, building a connection with 'residual connection'.

Often, the problem of polynomial filtering is reduced to learning a proper polynomial function in order  $K$ . The expressive power in terms of representing **arbitrary polynomial filters** has been discussed in former graph residual connection works, especially dense residues [1, 7]. However, motivated from the spatial view of

Permission to make digital or hard copies of all or part of this work for personal or classroom use is granted without fee provided that copies are not made or distributed for profit or commercial advantage and that copies bear this notice and the full citation on the first page. Copyrights for components of this work owned by others than ACM must be honored. Abstracting with credit is permitted. To copy otherwise, or republish, to post on servers or to redistribute to lists, requires prior specific permission and/or a fee. Request permissions from [permissions@acm.org](mailto:permissions@acm.org).

Conference'17, July 2017, Washington, DC, USA

© 2023 Association for Computing Machinery.

ACM ISBN 978-x-xxxx-xxxx-x/YY/MM...\$15.00

<https://doi.org/XXXXXXX.XXXXXXX>

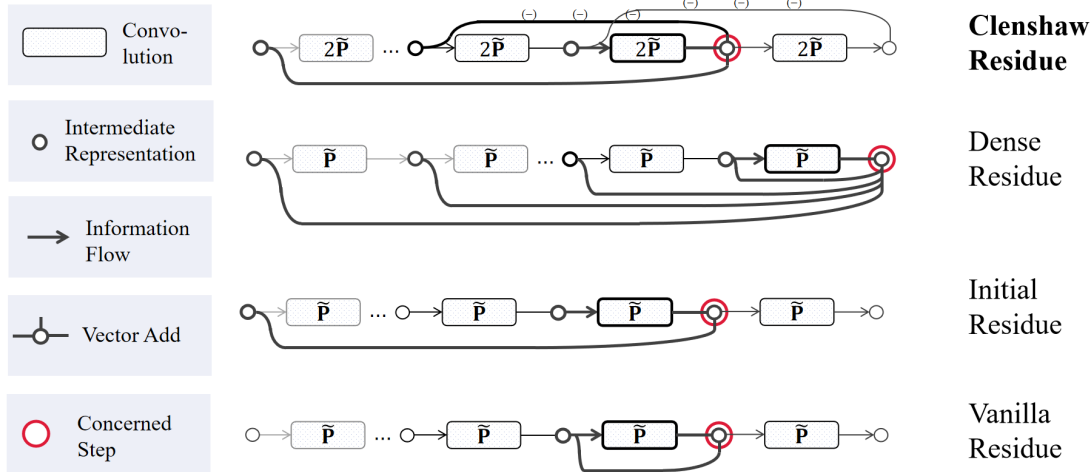


**Figure 1: Illustration of different graph residual connections. *Raw Residue* and *Initial Residue* follows a single-line structure, *Dense Residue* connect densely to all the former layers, while our *Clenshaw Residue* achieves strong expressive power by a neat double-line structure.**

message passing, these works lose an important part of spectral graph learning: the employe of **polynomial bases**. Polynomial bases are of considerable significance when learning filtering functions. Until now, different polynomial bases are utilized, including Chebyshev Basis [9, 14], Bernstein Basis [13] etc. See the example of Runge Phenomenon in [14] for an illustration of its importance.

*Contributions.* This paper focuses on the design of graph residual connections that exploit the expressive power of spectral polynomial filters. As we have demonstrated, raw residual connections and initial residual connections are primarily concerned with mitigating *over-smoothing*, and they commonly rely on the *homophily assumption*. Some dense residual connections do increase the expressive capacity of a GNN, with analyses aligning the spatial process with a potentially arbitrary spectral polynomial filter. Unfortunately, these works do not take the significance of different polynomial bases into account and are therefore incapable of learning a more effective spectral node representation.

In this paper, we introduce ClenshawGCN, a GNN model that employs the Clenshaw Summation Algorithm to enhance the expressiveness of the GCN model. More specifically, we list our contributions as follows:

- **Powerful residual connection submodules.** We propose ClenshawGCN, a message-passing GNN which borrows spectral power by adding two simple residual connection modules to each convolution layer: an *adaptive initial residue* and a *negative second order residue*;
- **Expressive power in terms of polynomial filters** We show that a  $K$ -order ClenshawGCN simulates *any*  $K$ -order polynomial function based on the *Chebyshev basis of the Second Kind*. More specifically, the *adaptive initial residue* allows for the flexibility of coefficients, while the *negative second order residue* allows for the

implicit use of Chebyshev basis. We prove this by the Clenshaw Summation Algorithm for Chebyshev basis (the Second Kind).

- **Outstanding performances.** We compare ClenshawGCN with both spatial and spectral models. Extensive empirical studies demonstrate that ClenshawGCN outperforms both spatial and spectral models on various datasets.

## 2 PRELIMINARIES

### 2.1 Notations

We consider a simple graph  $\mathcal{G} = (\mathcal{V}, \mathcal{E}, \mathbf{A})$ , where  $\mathcal{V} = \{1, 2, \dots, n\}$  is a finite node-set with  $|\mathcal{V}| = n$ ,  $\mathcal{E}$  is an edge-set with  $|\mathcal{E}| = m$ , and  $\mathbf{A}$  is an unnormalized adjacency matrix.  $\mathcal{L} = \mathbf{D} - \mathbf{A}$  denotes  $\mathcal{G}$ 's unnormalized graph Laplacian, where  $\mathbf{D} = \text{diag}\{d_1, \dots, d_n\}$  is the degree matrix with  $d_i = \sum_j \mathbf{A}_{ij}$ .

Following GCN, we add a self-connecting edge is to each node, and conduct symmetric normalization on  $\mathcal{L}$  and  $\mathbf{A}$ . The resulted *self-looped symmetric-normalized* adjacency matrix and Laplacian are denoted as  $\tilde{\mathbf{P}} = (\mathbf{D} + \mathbf{I})^{-1/2}(\mathbf{A} + \mathbf{I})(\mathbf{D} + \mathbf{I})^{-1/2}$  and  $\tilde{\mathcal{L}} = \mathbf{I} - \tilde{\mathbf{P}}$ , respectively.

Further, we attach each node with an  $f$ -dimensional raw feature and denote the feature matrix as  $\mathbf{X} \in \mathbb{R}^{n \times f}$ . Based on the the topology of underlying graph, GNNs enhance the raw node features to better representations for downstream tasks, such as node classification or link prediction.

### 2.2 Spatial Background

*Layer-wise Message Passing Architecture.* From a spatial view, the main body of a Graph Neural Network is a stack of *convolution* layers, who broadcast and aggregate feature information along the edges. Such a graph neural network is also called a Message Passing Neural Network (MPNN). To be concrete, we consider an MPNN

with  $K$  graph convolution layers and denote the nodes' representations of the  $\ell$ -th layer as  $\mathbf{H}^{(\ell)}$ .  $\mathbf{H}^{(\ell)}$  is constructed based on  $\mathbf{H}^{(\ell-1)}$  by an *propagation* and possibly a *transformation* operation. For example, in Vanilla GCN [18], the convolution layer is defined as

$$\mathbf{H}^{(\ell)} = \sigma(\tilde{\mathbf{P}}\mathbf{H}^{(\ell-1)}\mathbf{W}^{(\ell)}), \quad (1)$$

whose *propagation* operator is  $f : \mathbf{H}^{(\ell-1)} \rightarrow \tilde{\mathbf{P}}\mathbf{H}^{(\ell-1)}$  and *transformation* operator is  $f : \tilde{\mathbf{P}}\mathbf{H}^{(\ell-1)} \rightarrow \sigma(\tilde{\mathbf{P}}\mathbf{H}^{(\ell-1)}\mathbf{W}^{(\ell)})$ .

Extra transformations, or probably combinations, are applied before and after the stack of  $K$  convolution layers to form a map from  $\mathbf{X}$  to the final output  $\tilde{\mathbf{Y}}$ , which is determined by the downstream task, e.g.  $\mathbf{H}^{(0)} = \text{MLP}(\mathbf{X}; \mathbf{W}^{(0)})$  and  $\tilde{\mathbf{Y}} = \text{SoftMax}(\text{MLP}(\mathbf{H}^{(K)}; \mathbf{W}^{(K+1)}))$  for node classification tasks. In this paper, a slight difference in notation lies in that, we denote the input of convolution layers to be  $\mathbf{H}^*$ , instead of  $\mathbf{H}^{(0)}$ , and introduce notations  $\mathbf{H}^{(-1)}$  and  $\mathbf{H}^{(-2)}$  as zero matrices for simplicity of later representation.

*Entangled and Disentangled Architectures.* The motivations for *propagation* and *transformation* in a convolution layer differ. *Propagations* are related to graph topology, analyzed as an analog of walks [6, 19, 38, 42], diffusion processes [5, 20, 46], etc., while the *entangling of transformations* between *propagations* follows behind the convention of deep learning. A GNN is classified under a disentangled architecture if the *transformations* are disentangled from *propagations*, such as APPNP [19] and GPRGNN [7]. Though it is raised in [45] that the entangled architecture tends to cause model degradations, we observe that GCNII [6] under the entangled architecture does not suffer from this problem. So we follow the use of entangled transformations as in Vanilla GCN, and leverage the identity mapping of weight matrices as in GCNII.

### 2.3 Spectral Background

*Spectral Definition of Convolution.* Graph spectral domain leverages the geometric structure of underlying graphs in another way [35].

Conduct eigen-decomposition on  $\tilde{\mathcal{L}}$ , i.e.  $\tilde{\mathcal{L}} = \mathbf{U}\mathbf{\Lambda}\mathbf{U}^T$ , the spectrum  $\mathbf{\Lambda} = \text{diag}\{\lambda_1, \dots, \lambda_n\}$  is in non-decreasing order. Since  $\tilde{\mathcal{L}}$  is real-symmetric, elements in  $\mathbf{\Lambda}$  are real, and  $\mathbf{U}$  is a complete set of  $n$  orthonormal eigenvectors, which is used as a basis of *frequency components* analogously to *classic Fourier transform*.

Now consider a column in  $\mathbf{X}$  as a *graph signal* scattered on  $\mathcal{V}$ , denoted as  $\mathbf{x} \in \mathbb{R}^n$ . *Graph Fourier transform* is defined as  $\hat{\mathbf{x}} := \langle \mathbf{U}, \mathbf{x} \rangle = \mathbf{U}^T \mathbf{x}$ , which projects graph signal  $\mathbf{x}$  to the *frequency responses* of basis components  $\hat{\mathbf{x}}$ . It is then followed by *modulation*, which can be presented as  $\hat{\mathbf{x}}^* := g_\theta \hat{\mathbf{x}} = \text{diag}\{\theta_1, \dots, \theta_n\} \hat{\mathbf{x}}$ . After modulation, *inverse Fourier transform*:  $\mathbf{x}^* := \mathbf{U} \hat{\mathbf{x}}^*$  transform  $\hat{\mathbf{x}}^*$  back to the spatial domain. The three operations form a spectral definition of *convolution*:

$$g_\theta \star \mathbf{x} = \mathbf{U} g_\theta \mathbf{U}^T \mathbf{x}, \quad (2)$$

which is also called *spectral filtering*. Specifically, when  $\theta_i = 1 - \lambda_i$ ,  $\mathbf{U} g_\theta \mathbf{U}^T \mathbf{x} \equiv \tilde{\mathbf{P}} \mathbf{x}$ , giving an spectral explanation of GCN's convolution in Equation (1).

*Polynomial Filtering.* The calculation of  $\mathbf{U}$  in Equation (2) is of prohibitively expensive. To avoid explicit eigen-decomposition of  $\mathbf{U}$ ,  $g_\theta$

is often defined as a polynomial function of a frequency component's corresponding eigenvalue parameterized by  $\theta$ , that is,

$$\hat{\mathbf{x}}_i^* = g_\theta(\lambda_i) \langle \mathbf{U}_i, \mathbf{x} \rangle.$$

The spectral filtering process then becomes

$$g_\theta \star \mathbf{x} = \mathbf{U} g_\theta(\mathbf{\Lambda}) \mathbf{U}^T \mathbf{x} \equiv g_\theta(\tilde{\mathcal{L}}) \mathbf{x}, \quad (3)$$

where  $g_\theta(\tilde{\mathcal{L}}) \mathbf{x}$  eliminates eigen-decomposition and can be calculated in a localized way in  $\mathcal{O}(|\mathcal{E}|)$  [9, 18].

*Definition 2.1 (Polynomial Filters).* Consider a graph whose Laplacian matrix is  $\tilde{\mathcal{L}}$  and use the set of orthonormal eigenvectors of  $\tilde{\mathcal{L}}$  as the frequency basis, a **polynomial filter** is a process that scales each frequency component of the input signal by  $g_\theta(\lambda)$ , where  $g_\theta$  is a polynomial function and  $\lambda$  is the corresponding eigenvalue of the frequency component.

Equivalently, we can define the filtering function on the spectrum of  $\tilde{\mathbf{P}}$ , instead of  $\tilde{\mathcal{L}}$ . Since  $\tilde{\mathbf{P}} = \mathbf{I} - \tilde{\mathcal{L}}$ ,  $\tilde{\mathbf{P}}$  and  $\tilde{\mathcal{L}}$  share the same set of orthonormal eigenvectors  $\mathbf{U}$ , and the spectrum of  $\tilde{\mathbf{P}}$ , denoted as  $\mathbf{M} = \{\mu_1, \dots, \mu_n\}$ , satisfies  $\mu_i = 1 - \lambda_i$  ( $i = 1, \dots, n$ ). Thus, the filtering function can be defined as  $h_\theta$ , where

$$h_\theta(\mu) \equiv g_\theta(1 - \mu). \quad (4)$$

In Section 3, for the brevity of presentation, we will use this equivalent definition.

### 2.4 Polynomial Approximation and Chebyshev Polynomials

*Polynomial Approximation.* Following the idea of polynomial filtering (Equation (3)), the problem then becomes the approximation of polynomial  $g_\theta$ . A line of work approximates  $g_\theta$  by some truncated polynomial basis  $\{\phi_i(x)\}_{i=0}^{i=K}$  up to the  $K$ -th order, i.e.

$$g_\theta(x) = \sum_{k=0}^K \theta_k \phi_k(x),$$

where  $\vec{\theta} = [\theta_0, \dots, \theta_K] \in \mathbb{R}^{K+1}$  is the coefficients. In the field of polynomial filtering and spectral GNNs, different bases have been explored for  $\{\phi_i(x)\}_{i=0}^{i=K}$ , including Chebyshev basis [9], Bernstein basis [13], Jacobi basis [39], etc.

*Chebyshev Polynomials.* Chebyshev basis has been explored since early attempts for the approximation of  $g_\theta$  [9]. Besides Chebyshev polynomials of the first kind ( $\{T_i(x)\}_{i=0}^{\infty}$ ), the second kind ( $\{U_i(x)\}_{i=0}^{\infty}$ ) is also widely used.

Both  $\{T_i(x)\}_{i=0}^{\infty}$  and  $\{U_i(x)\}_{i=0}^{\infty}$  can be generated by a *recurrence relation*:

$$\begin{aligned} T_0(x) &= 1, & T_1(x) &= x, \\ T_n(x) &= 2xT_{n-1}(x) - T_{n-2}(x). \quad (n = 2, 3, \dots) \end{aligned}$$

$$\begin{aligned} U_{-1}(x) &= 0, & U_0(x) &= 1, & U_1(x) &= 2x, \\ U_n(x) &= 2xU_{n-1}(x) - U_{n-2}(x). \quad (n = 1, 2, \dots) \end{aligned} \quad (5)$$

The recurrence relation is used in ChebyNet [9] for accelerating the computing of polynomial filtering. Note that we start the second kind from  $U_{-1}$ , which will be used in later proof in Section 3.3.

## 2.5 Residual Network Structures

We have discussed some graph residual connections in Introduction. In this section, we list some model in detail for illustration of residual connections.

**GCNII** equips the vanilla GCN convolution with two techniques: initial residue and identity mapping:

$$\mathbf{H}^{(\ell)} = \sigma \left( (1-\alpha) \tilde{\mathbf{P}} \mathbf{H}^{(\ell-1)} + \alpha \mathbf{H}^* \right) \left( (1-\beta_\ell) \mathbf{I}_n + \beta_\ell \mathbf{W}^{(\ell)} \right). \quad (6)$$

Ignoring non-linear transformation, GCNII iteratively solves the optimization problem:

$$\arg \min_{\mathbf{H}} \alpha \|\mathbf{H} - \mathbf{H}^*\|_F^2 + (1-\alpha) \text{tr} \left( \mathbf{H}^\top \tilde{\mathcal{L}} \mathbf{H} \right). \quad (7)$$

The optimization goal reveals the underlying *homophily assumption*, where initial residual connection is only making a *compromise* between Laplacian smoothing and keeping identity.

**AirGNN** [24] proposes an extension for initial residue, where the first term of optimization problem in Equation (7) is replaced by the  $\ell_{21}$  norm. By solving the optimization problem, AirGNN adaptively choose  $\alpha$ . However, limited by the optimization goal, AirGNN still falls into the homophily assumption.

**JKNet** [42] uses dense residual connection at the last layer and combine all the intermediate representations nodewise by different ways, including LSTM, Max-Pooling and so on.

**MixHop** [1] concats feature maps of several hops at each layer, represented as

$$\mathbf{H}^{(\ell+1)} = \left\| \left\| \sigma \left( \tilde{\mathbf{P}}^j \mathbf{H}^{(\ell)} \mathbf{W}_j^{(\ell)} \right), \right. \right. \\ \left. \left. j \in K \right. \right.$$

which can be considered as staking several dense graph residual networks.

## 3 METHOD

### 3.1 Clenshaw Convolution

We formulate the  $\ell$ -th layer's representation of ClenshawGCN as

$$\mathbf{H}^{(\ell)} = \sigma \left( \left( 2\tilde{\mathbf{P}} \mathbf{H}^{(\ell-1)} - \mathbf{H}^{(\ell-2)} + \alpha_\ell \mathbf{H}^* \right) \left( (1-\beta_\ell) \mathbf{I}_n + \beta_\ell \mathbf{W}^{(\ell)} \right) \right), \quad (8)$$

where  $\ell = 0, 1, \dots, K$ ,  $\mathbf{H}^{(-2)} = \mathbf{H}^{(-1)} = \mathbf{O}$ ,  $\mathbf{H}^* = \text{MLP}(\mathbf{X}; \mathbf{W}^*)$ .

Note that for *transformation*, we use identity mapping with  $\beta_\ell = \log(\frac{\lambda}{\ell} + 1) \approx \lambda/\ell$  following GCNII [6]. Comparing to GCNII, we include two simple yet effective residual connections: **Adaptive Initial Residue** and **Negative Second Order Residue**:

$$2\tilde{\mathbf{P}} \mathbf{H}^{(\ell-1)} \quad \underbrace{-\mathbf{H}^{(\ell-2)}}_{\text{Negative Second Order Residue}} \quad + \quad \underbrace{\alpha_\ell \mathbf{H}^*}_{\text{Adaptive Initial Residue}}.$$

In the remaining part of this section, we will illustrate the role and mechanism of these two residual modules. In summary, *adaptive initial residue* enables the simulating of any  $K$ -order polynomial

filter, while *negative second order residue*, motivated by the leveraging of 'differencing relations', simulates the use of Chebyshev basis in the approximation of filtering functions. For both two parts, we will give an intuitive analysis with followed by a proofs.

### 3.2 Adaptive Initial Residue

The role of *adaptive initial residue* is to enable the expressive power of any  $K$ -order polynomial filter. To illustrate this, we will first consider an **incomplete** version of the ClenshawGCN termed HornerGCN.

*Intuition.* We start with an analysis of GCNII. To simplify the analysis, we consider  $(1-\beta_\ell) \mathbf{I}_n + \beta_\ell \mathbf{W}^{(\ell)}$  as  $\mathbf{I}$ , and take  $\text{relu}(x) = x$ . At this point, the iteration (6) is simplified as

$$\mathbf{H}^{(\ell)} = (1-\alpha) \tilde{\mathbf{P}} \mathbf{H}^{(\ell-1)} + \alpha \mathbf{H}^*. \quad (9)$$

Consider a GCNII model of order  $K^1$ , by expanding (9), we obtain that

$$\mathbf{H}^{(K)} = \sum_{\ell=0}^K \hat{\alpha}_\ell \tilde{\mathbf{P}}^\ell \mathbf{H}^*, \quad (10)$$

where

$$\hat{\alpha}_\ell = \begin{cases} \alpha(1-\alpha)^\ell, & \ell < K, \\ (1-\alpha)^K, & \ell = K. \end{cases}$$

It can be seen that the iterative process of GCNII implicitly leverages the representations of different layers with *fixed* and *positive* coefficients. However, we want *flexible* exploitation of different diffusion layers, [42, 46]. More importantly, we need to have *negative* weights in cases of heterophilic graphs [7]. To this end, we can simply replace the fixed  $\alpha$  in (6) with *learnable* ones. In this way, we obtain the form of HornerGCN as follows,

$$\mathbf{H}^{(\ell)} = \sigma \left( \left( \tilde{\mathbf{P}} \mathbf{H}^{(\ell-1)} + \alpha_\ell \mathbf{H}^* \right) \left( (1-\beta_\ell) \mathbf{I}_n + \beta_\ell \mathbf{W}^{(\ell)} \right) \right), \quad (11)$$

where  $\ell = 0, 1, \dots, K$ ,  $\mathbf{H}^{(-1)} = \mathbf{O}$ ,  $\mathbf{H}^* = \text{MLP}(\mathbf{X}; \mathbf{W}^*)$ .

*Spectral Nature.* With the definition of *polynomial filters* given in Equation (4) and Definition 2.1, we will prove the Theorem below:

**THEOREM 3.1.** *A  $K$ -order HornerGCN defined in Equation (11), when consider  $(1-\beta_\ell) \mathbf{I}_n + \beta_\ell \mathbf{W}^{(\ell)}$  for each  $\ell$  as  $\mathbf{I}$ , and  $\text{relu}(x)$  as  $x$ , simulates a polynomial filter on the monomial basis:*

$$h(\mu) = \sum_{\ell=0}^K \alpha_{K-\ell} \mu^\ell,$$

where  $\{\alpha_\ell\}_{\ell=0}^K$  is the set of initial residue coefficients.

*Horner's Method.* To prove Theorem 3.1, we first briefly introduce Horner's Method [15]. Given  $p(x) = \sum_{i=0}^n a_i x^i = a_0 + a_1 x + \dots + a_n x^n$ , Horner's Method is a classic method for evaluating  $p(x_0)$ , by viewing  $p(x)$  as the following form:

$$p(x) = a_0 + x (a_1 + x (a_2 + x (a_3 + \dots + x (a_{n-1} + x a_n) \dots))). \quad (12)$$

<sup>1</sup>For simplicity, we term a model with at most  $K$  propagations as of order  $K$

Thus, Horner's method defines a recursive method for evaluating  $p(x_0)$ :

$$\begin{aligned} b_n &:= a_n, \\ b_{n-1} &:= a_{n-1} + b_n x_0, \\ &\dots \\ b_0 &:= a_0 + b_1 x_0, \\ p(x_0) &:= b_0. \end{aligned} \quad (13)$$

*Proof of Spectral Expressiveness.* Note that the form of Horner's recursive are parallel with the recursive of stacked Horner convolutions by ignoring the non-linear transformations. Thus, by unfolding the nested expression of Horner convolutions (11), we get the output of the last layer closely matched with the form of Equation (12) :

$$\begin{aligned} \mathbf{H}^{(0)} &= \alpha_0 \mathbf{H}^*, \\ \mathbf{H}^{(1)} &= \tilde{\mathbf{P}}(\alpha_0 \mathbf{H}^*) + \alpha_1 \mathbf{H}^*, \\ &\dots \\ \mathbf{H}^{(K)} &= \tilde{\mathbf{P}}\left(\dots\left(\tilde{\mathbf{P}}\left(\tilde{\mathbf{P}}(\alpha_0 \mathbf{H}^*) + \alpha_1 \mathbf{H}^*\right) + \alpha_2 \mathbf{H}^*\right)\dots\right) + \alpha_K \mathbf{H}^* \\ &= \alpha_K \mathbf{H}^* + \alpha_{K-1} \tilde{\mathbf{P}} \mathbf{H}^* + \dots + \alpha_0 \tilde{\mathbf{P}}^K \\ &= \sum_{\ell=0}^K \alpha_{K-\ell} \tilde{\mathbf{P}}^\ell \mathbf{H}^*. \end{aligned} \quad (14)$$

So, the final representation

$$\mathbf{H}^{(K)} = \sum_{\ell=0}^K \alpha_{K-\ell} \tilde{\mathbf{P}}^\ell \mathbf{H}^* = \mathbf{U} \left( \sum_{\ell=0}^K \alpha_{K-\ell} \mathbf{M}^\ell \right) \mathbf{U}^T \mathbf{H}^*,$$

corresponds to the result of a polynomial filter  $h$  on the spectrum of  $\tilde{\mathbf{P}}$ , where

$$h(\mu) = \sum_{\ell=0}^K \alpha_{K-\ell} \mu^\ell.$$

### 3.3 Negative Second Order Residue

The role of *negative second order residue* is to enable the leverage of Chebyshev basis. Compared with the adaptive initial residue, it is not obvious. In this section, we will first give an **intuitive** motivation for Negative Second Order Residue, and then reveal the mechanism behind it by Clenshaw Summation Algorithm.

*Intuition of Taking Difference.* There is already some work that has noticed the 'subtraction' relationship between progressive levels of representation [1, 43]. For example, one of MixHop's direct challenges towards the traditional GCN model is the inability to represent the *Delta Operator*, i.e.,  $\mathbf{A}\mathbf{X}^2 - \mathbf{A}\mathbf{X}$ , which is an important relationship in representing both the concept of social boundaries [30] and the concept of 'sharpening' in images [4, 28].

Instead of considering model's ability to represent *Delta Operator* in the final output, we take a more direct use of these difference relations. That is, we add  $\tilde{\mathbf{P}}\mathbf{H}^{(\ell-1)} - \mathbf{H}^{(\ell-2)}$  to each convolution

layers of (11), and get the final form of Clenshaw Convolution:

$$\tilde{\mathbf{P}}\mathbf{H}^{(\ell-1)} + \alpha_\ell \mathbf{H}^* + \tilde{\mathbf{P}}\mathbf{H}^{(\ell-1)} - \mathbf{H}^{(\ell-2)} \implies (8).$$

A question that perhaps needs to be answered is: why not instead insert a more direct difference relation:  $\tilde{\mathbf{P}}\mathbf{H}^{(\ell-1)} - \mathbf{H}^{(\ell-1)}$ ? The reason is, at this point, the convolution would become

$$\tilde{\mathbf{P}}\mathbf{H}^{(\ell-1)} + \alpha_\ell \mathbf{H}^* + \tilde{\mathbf{P}}\mathbf{H}^{(\ell-1)} - \mathbf{H}^{(\ell-1)} = (2\tilde{\mathbf{P}} - \mathbf{I}) \mathbf{H}^{(\ell-1)} + \alpha_\ell \mathbf{H}^*,$$

whose unfolded form, by substitute  $\tilde{\mathbf{P}}$  to  $2\tilde{\mathbf{P}} - \mathbf{I}$  in (14), would become  $\sum_{\ell=0}^K \alpha_{K-\ell} (2\tilde{\mathbf{P}} - \mathbf{I})^\ell \mathbf{H}^*$ , which brings limited change.

*Spectral Nature.* Besides the spatial intuition of considering sub-stractions or boundaries, we reveal the spectral nature of our *negative residual connection* in this part, that is, it simulates the leverage of chebyshev basis as in spectral polynomials. With the definition of *polynomial filters* given in Equation (4) and Definition 2.1, we will prove the theorem below:

**THEOREM 3.2.** *A  $K$ -order ClenshawGCN defined in Equation (8), when consider  $(1 - \beta_\ell)\mathbf{I}_n + \beta_\ell \mathbf{W}^{(\ell)}$  for each  $\ell$  as  $\mathbf{I}$ , and  $\text{relu}(x)$  as  $x$ , simulates a polynomial filter*

$$h(\mu) = \sum_{\ell=0}^K \alpha_{K-\ell} U_\ell(\mu),$$

where  $\{U_\ell\}_{\ell=0}^K$  is the truncated  $K$ -order second-kind Chebyshev basis, and  $\{\alpha_\ell\}_{\ell=0}^K$  is the set of initial residue coefficients.

which can also be expressed as:

$$\mathbf{H}^{(K)} = \mathbf{U}h(\mathbf{M})\mathbf{U}^T \mathbf{H}^* = \mathbf{U} \left( \sum_{\ell=0}^K \alpha_{K-\ell} U_\ell(\mathbf{M}) \right) \mathbf{U}^T \mathbf{H}^*. \quad (15)$$

*Clenshaw Algorithm.* For the proof of Theorem 3.2, we will first introduce Clenshaw Summation Algorithm as a Corollary.

**COROLLARY 3.3 (CLENSHAW SUMMATION ALGORITHM FOR CHEBYSHEV POLYNOMIALS (SECOND KIND)).** *For the Second Kind of Chebyshev Polynomials, the weighted sum of a finite series of  $\{U_k(x)\}_{k=0}^n$ :*

$$S(x) = \sum_{k=0}^{k=n} a_k U_k(x)$$

can be computed by a recurrence formula:

$$\begin{aligned} b_{n+2}(x) &:= 0, \\ b_{n+1}(x) &:= 0, \\ b_k(x) &:= a_k + 2x b_{k+1}(x) - b_{k+2}(x). \end{aligned} \quad (k = n, n-1, \dots, 0) \quad (16)$$

Then  $S(x) \equiv b_0(x)$ .

Clenshaw Summation can be applied to a wider range of polynomial basis. However, specifically for the second kind of Chebyshev,

we made some slight simplifications<sup>2</sup>, so for clarity of discussion, we give the proof here.

PROOF FOR COROLLARY 3.3. Denote

$$A = \begin{bmatrix} 1 & & & & \\ -2x & 1 & & & \\ 1 & -2x & 1 & & \\ & & \dots & & \\ & & & 1 & -2x & 1 \end{bmatrix}, \quad \vec{u} = \begin{bmatrix} U_{-1}(x) \\ U_0(x) \\ U_1(x) \\ \dots \\ U_n(x) \end{bmatrix}, \quad \vec{a} = \begin{bmatrix} 0 \\ a_0 \\ a_1 \\ \dots \\ a_n \end{bmatrix},$$

with  $A \in \mathbb{R}^{(n+2) \times (n+2)}$ ,  $\vec{u} \in \mathbb{R}^{n+2}$ , then

$$S(x) = \vec{a}^T \vec{u}. \quad (17)$$

Indexing a vector from  $-1$ , we denote  $\mathbf{1}_i \in \mathbb{R}^{(n+2)}$  as the one-hot vector with the  $i$ -th element being 1 ( $i$  starts from  $-1$ ). Note that, since the recurrence relation for the Chebyshev polynomials (5),

$$A\vec{u} = \begin{bmatrix} U_{-1}(x) \\ -2xU_{-1}(x) + U_0(x) \\ 0 \\ \dots \\ 0 \end{bmatrix} = \begin{bmatrix} 0 \\ U_0(x) \\ 0 \\ \dots \\ 0 \end{bmatrix} = \mathbf{1}_0. \quad (18)$$

Now suppose that there is a vector  $\vec{b} = [b_{-1}, b_0, \dots, b_n]$  satisfying

$$\vec{a}^T = \vec{b}^T A, \quad (19)$$

then

$$S(x) \stackrel{(17)}{=} \vec{a}^T \vec{u} \stackrel{(19)}{=} \vec{b}^T A\vec{u} \stackrel{(18)}{=} \vec{b}^T \mathbf{1}_0 = b_0.$$

On the other hand, notice that the recurrence defined in (16) is exactly the Gaussian Elimination process of solving  $\vec{a}^T = \vec{b}^T A$  from  $b_n$  down to  $b_0$ , which means that  $\{b_n, \dots, b_0\}$  calculated by (16) satisfies (19). Proof for Corollary 3.3 is finished.  $\square$

*Proof of Spectral Expressiveness.* Now we prove Theorem 3.2 inductively based on Corollary 3.3.

PROOF OF THEOREM 3.2. **Given:**

$$\mathbf{H}^{(\ell)} = 2\tilde{\mathbf{P}}\mathbf{H}^{(\ell-1)} - \mathbf{H}^{(\ell-2)} + \alpha_\ell \mathbf{H}^*, \quad (20)$$

$$\mathbf{H}^{(-1)} = \mathbf{H}^{(-2)} = \mathbf{0}.$$

**Induction Hypothesis:** Suppose that when the convolutions have processed to the  $\ell$ -th layer,  $\mathbf{H}^{(\ell-1)}$  and  $\mathbf{H}^{(\ell-2)}$  are already proved to be polynomial filtered results of  $\mathbf{H}^*$ , we show that  $\mathbf{H}^{(\ell)}$  is also polynomial filtered results of  $\mathbf{H}^*$ .

Further, denote the polynomial filtering functions of generating  $\mathbf{H}^{(\ell-2)}$ ,  $\mathbf{H}^{(\ell-1)}$  and  $\mathbf{H}^{(\ell)}$  to be  $h^{(\ell-2)}$ ,  $h^{(\ell-1)}$  and  $h^{(\ell)}$ . Then  $h^{(\ell)}$  satisfies:

$$h^{(\ell)}(\mu) = \alpha_\ell + 2\mu h^{(\ell-1)}(\mu) - h^{(\ell-2)}(\mu).$$

**Base Case:** For  $\ell = 0$ , since  $\mathbf{H}^{(-2)} = \mathbf{H}^{(-1)} = \mathbf{0}$ ,  $\mathbf{H}^{(0)} = \alpha_0 \mathbf{H}^*$ , the first induction step is established with

$$h^{(0)}(\mu) = \alpha_0, \quad h^{(-1)}(\mu) = 0, \quad h^{(-2)}(\mu) = 0.$$

<sup>2</sup>To be more precise, the simplification lies in that Clenshaw Summation procedures for the more general situation need an 'extra' different step which is not needed in our proof.

**Induction Step:** Insert

$$\begin{cases} \mathbf{H}^{(\ell-1)} &= \mathbf{U}h^{(\ell-1)}(\mathbf{M})\mathbf{U}^T\mathbf{H}^*, \\ \mathbf{H}^{(\ell-2)} &= \mathbf{U}h^{(\ell-2)}(\mathbf{M})\mathbf{U}^T\mathbf{H}^*, \\ \tilde{\mathbf{P}} &= \mathbf{U}\mathbf{M}\mathbf{U}^T \end{cases}$$

into Equation (20), we get

$$\begin{aligned} \mathbf{H}^{(\ell)} &= 2\mathbf{U}\mathbf{M}\mathbf{U}^T\mathbf{U}h^{(\ell-1)}(\mathbf{M})\mathbf{U}^T\mathbf{H}^* - \mathbf{U}h^{(\ell-2)}(\mathbf{M})\mathbf{U}^T\mathbf{H}^* + \alpha_\ell \mathbf{H}^* \\ &= \mathbf{U} \left( \alpha_\ell + 2\mathbf{M}h^{(\ell-1)}(\mathbf{M}) - h^{(\ell-2)}(\mathbf{M}) \right) \mathbf{U}^T \mathbf{H}^*. \end{aligned}$$

So,  $\mathbf{H}^{(\ell)}$  is also a polynomial filtered result of  $\mathbf{H}^*$ , with filtering function  $h^{(\ell)}$ :

$$h^{(\ell)}(\mu) := \alpha_\ell + 2\mu h^{(\ell-1)}(\mu) - h^{(\ell-2)}(\mu). \quad (21)$$

Stack relation(21) for  $\ell = 0, 1, \dots, K$ , we get:

$$\begin{aligned} h^{(-2)}(\mu) &= 0, \\ h^{(-1)}(\mu) &= 0, \\ h^{(\ell)}(\mu) &:= \alpha_\ell + 2\mu h^{(\ell-1)}(\mu) - h^{(\ell-2)}(\mu), \\ &\quad (k = 0, 1, \dots, K). \end{aligned}$$

where the progressive access of  $b^{(\ell)}$  is in a **totally parallel** way with the recurrence (16) in Clenshaw Summation Algorithm. We soonly get

$$\sum_{\ell=0}^K \alpha_{K-\ell} U_\ell(\mu) \equiv h^{(K)}(\mu).$$

Thus, we have finished the proof of Theorem 3.2.  $\square$

## 4 EXPERIMENTS

In this section, we conduct two sets of experiments with the node classification task. First, we verify the power of our method by comparing it with both spatial residual methods and powerful spectral models. Second, we verify the effectiveness of the two submodules by ablation studies.

### 4.1 Experimental Setup

*Datasets and Splits.* We use both homophilic graphs and heterophilic graphs in our experiments following former works, especially GCN [18], Geom-GCN [29] and LINKX [23].

- *Citation Graphs.* Cora, PubMed, and CiteSeer are citation datasets [34] processed by Planetoid [44]. In these graphs, nodes are scientific publications, edges are citation links processed to be bidirectional, and node features are bag-of-words representations of the documents. These graphs show strong homophily.
- *Wikipedia Graphs.* Chameleon dataset and Squirrel dataset are page-page networks on topics in Wikipedia, where nodes are entries, and edges are mutual links.
- *Webpage Graphs.* Texas dataset and Cornell dataset collect web pages from computer science departments of different universities. The nodes in the graphs are web pages of students, projects, courses, staff or faculties [8], the edges are hyperlinks between them, and node features are the bag-of-words representations of these web pages.

- *Co-occurrence Network*. The Actor network represents the co-occurrence of actors on a Wikipedia page [37]. The node features are filtered keywords in the Wikipedia pages. The categorization of the nodes is done by [29].
- *Mutual follower Network*. Twitch-Gamers dataset represents the mutual following relationship between accounts on the streaming platform Twitch.

We list the messages of these networks in Table 1, where  $\mathcal{H}(G)$  is the measure of homophily in a graph proposed by Geom-GCN [29]. Larger  $\mathcal{H}(G)$  implies stronger homophily.

**Table 1: Statistics for the node classification datasets we use. Datasets of different homophily degrees are used.**

Dataset	#Nodes	#Edges	#Classes	$\mathcal{H}(G)$
Cora	2,709	5,429	7	.83
Pubmed	19,717	44,338	3	.71
Citeseer	3,327	4,732	6	.79
Squirrel	5,201	217,073	5	.22
Chameleon	7,600	33,544	5	.23
Texas	183	309	5	.11
Cornell	183	295	5	.30
Twitch-Gamers	168,114	6,797,557	7	.55

For all datasets except for the Twitch-gamers dataset, we take a 60%/20%/20% train/validation/test split proportion following former works [7, 13, 14, 29]. We run these datasets twenty times over random splits with random initialization seeds. For the Twitch-gamers dataset, we use the five random splits given in LINKX [23] with a 50%/25%/25% proportion to align with reported results.

*ClenshawGCN Setup*. Before and after the stack of Clenshaw convolution layers, two non-linear transformations are made to link with the dimensions of the raw features and final class numbers. All the intermediate transformation layers are set with 64 hidden units. For the initialization of the adaptive initial residues’ coefficients, denoted as  $\vec{\alpha} = [\alpha_0, \dots, \alpha_K]$ , we simply set  $\alpha_K$  to be 1 and all the other coefficients to be 0, which corresponds to initializing the polynomial filter to be  $g(\lambda) = 1$  (or equivalently,  $h(\mu) = 1$ ).

*Hyperparameter Tuning*. For the optimization process on the training sets, we tune  $\vec{\alpha}$  with SGD optimizer with momentum [36] and all the other parameters with Adam SGD [17]. We use early stopping with a patience of 300 epochs.

For the search space of hyperparameters, below is the search space of hyperparameters:

- Orders of convolutions:  $K \in \{8, 12, \dots, 32\}$ ;
- Learning rates:  $\{0.001, 0.005, 0.1, 0.2, 0.3, 0.4, 0.5\}$ ;
- Weight decays:  $\{1e-8, 1e-7, \dots, 1e-3\}$ ;
- Dropout rates:  $\{0, 0.1, \dots, 0.7\}$ .

We tune all the hyperparameters on the validation sets. To accelerate hyperparameter searching, we use Optuna [2] and run 100 completed trials<sup>3</sup> for each dataset.

<sup>3</sup>In Optuna, a *trial* means a run with hyperparameter combination; the term ‘complete’ refers to that, some trials of bad expectations would be pruned before completion.

## 4.2 Comparing ClenshawGCN with Other Graph Residual Connections

In this subsection, we illustrate the effectiveness of ClenshawGCN’s residual connections by comparing ClenshawGCN with other spatial models, including GCNII [6], H<sub>2</sub>GCN [48], MixHop [1] and JKNet [42]. Among them, GCNII is equipped with initial residual connections, and the others are equipped with dense residual connections. Moreover, the way of combining multi-scale representations is more complex than weighted sum in H<sub>2</sub>GCN and JKNet. As shown in Table 2, our ClenshawGCN outperforms all the baselines.

On one hand, in line with our expectations, ClenshawGCN outperforms all the baselines on the *heterophilic datasets* by a significantly large margin including H<sub>2</sub>GCN, which is tailored for heterophilic graphs. This illustrates the effectiveness of borrowing spectral characteristics.

On the other hand, ClenshawGCN even shows an advantage over *homophilic datasets*, though the compared spatial models, such as GCNII and JKNet, are strong baselines on such datasets. Especially, for the PubMed dataset, ClenshawGCN achieves state of art.

## 4.3 Comparing ClenshawGCN with Spectral Baselines

In Section 3.3, we have proved that ClenshawGCN acts as a spectral model and simulates any  $K$ -order polynomial filter based on  $\{U_\ell\}_{\ell=0}^{\ell=K}$ . In this subsection, we compare ClenshawGCN with strong spectral GNNs, including ChebNet [9], APPNP [19], ARMA [3], GPRGNN [7], BernNet [13], and ChebNetII [14]. Among them, APPNP simulates polynomial filters with *fixed* parameters, ARMA GNN simulates ARMA filters [27], and the rest simulate *learnable* polynomial filters based on the Chebyshev basis, Monomial basis or Bernstein basis.

As reported in Table 3, ClenshawGCN outperforms almost all the baselines on each dataset, except for Chameleon and Citeseer. Specifically, ClenshawGCN outperforms other models on the Squirrel dataset by a large margin of 7.66%.

Note the comparison between ClenshawGCN and ChebNetII. ChebNetII gains *extra power* from the leveraging of Chebyshev nodes, which is crucial for polynomial interpolation. However, without the help of Chebyshev nodes, ClenshawGCN is comparable to ChebNetII in performance. The extra power of ClenshawGCN may come from the entangled non-linear transformations.

## 4.4 Ablation Analysis

For ClenshawGCN, the core of the design is the two residual connection modules. In this section, we conduct ablation analyses on these two modules to verify their contribution.

*Ablation Model: HornerGCN*. We use HornerGCN as an ablation model to verify the contribution of *negative residues*. Recal Theorem 3.1, the corresponding polynomial filter of HornerGCN is

$$h_{\text{Horner}}(\mu) = \sum_{\ell=0}^K \alpha_{K-\ell} \mu^\ell,$$

which uses the Monomial basis. While the complete form of our ClenshawGCN borrows the use of chebyshev basis by negative residues.

**Table 2: Comparison with other models equipped by different kinds of residual connections. Mean classification accuracies ( $\pm$  standard derivation) of random splits are displayed. Besides the ClenshawGCN, all the results are taken directly from [25] and [23]. For the Twitch-Gamer dataset, we use 5 fixed 50%/25%/25% splits given in [23] to align with the reported results. For all the other datasets, 20 random 60%/20%/20% splits were used. (M) denotes some hyperparameter settings run out of memory [23].**

Datasets	Chameleon	Squirrel	Actor	Texas	Cornell	Cora	Citeseer	Pubmed	Twitch-gamer
$ \mathcal{V} $	2,277	5,201	7,600	183	183	2,708	3,327	19,717	168,114
MLP	46.59 $\pm$ 1.84	31.01 $\pm$ 1.18	40.18 $\pm$ 0.55	86.81 $\pm$ 2.24	84.15 $\pm$ 3.05	76.89 $\pm$ 0.97	76.52 $\pm$ 0.89	86.14 $\pm$ 0.25	60.92 $\pm$ 0.07
GCN	60.81 $\pm$ 2.95	45.87 $\pm$ 0.88	33.26 $\pm$ 1.15	76.97 $\pm$ 3.97	65.78 $\pm$ 4.16	87.18 $\pm$ 1.12	79.85 $\pm$ 0.78	86.79 $\pm$ 0.31	62.18 $\pm$ 0.26
GCNII	63.44 $\pm$ 0.85	41.96 $\pm$ 1.02	36.89 $\pm$ 0.95	80.46 $\pm$ 5.91	84.26 $\pm$ 2.13	88.46 $\pm$ 0.82	79.97 $\pm$ 0.65	89.94 $\pm$ 0.31	63.39 $\pm$ 0.61
H <sub>2</sub> GCN	52.30 $\pm$ 0.48	30.39 $\pm$ 1.22	38.85 $\pm$ 1.17	85.90 $\pm$ 3.53	86.23 $\pm$ 4.71	87.52 $\pm$ 0.61	79.97 $\pm$ 0.69	87.78 $\pm$ 0.28	(M)
MixHop	36.28 $\pm$ 10.22	24.55 $\pm$ 2.60	33.13 $\pm$ 2.40	76.39 $\pm$ 7.66	60.33 $\pm$ 28.53	65.65 $\pm$ 11.31	49.52 $\pm$ 13.35	87.04 $\pm$ 4.10	65.64 $\pm$ 0.27
GCN+JK	64.68 $\pm$ 2.85	53.40 $\pm$ 1.90	32.72 $\pm$ 2.62	80.66 $\pm$ 1.91	66.56 $\pm$ 13.82	86.90 $\pm$ 1.51	73.77 $\pm$ 1.85	90.09 $\pm$ 0.68	63.45 $\pm$ 0.22
ClenshawGCN	<b>69.44<math>\pm</math>2.06</b>	<b>62.14<math>\pm</math>1.65</b>	<b>42.08<math>\pm</math>1.99</b>	<b>93.36<math>\pm</math>2.35</b>	<b>92.46<math>\pm</math>3.72</b>	<b>88.90<math>\pm</math>1.26</b>	<b>80.34<math>\pm</math>1.26</b>	<b>91.99<math>\pm</math>0.41</b>	<b>66.26<math>\pm</math>0.27</b>

**Table 3: Comparison with spectral models. Mean classification accuracies ( $\pm$ 95% confidence intervals) on 20 random 60%/20%/20% train/validation/test splits are displayed. Besides the ClenshawGCN, all the results are taken directly from [13].**

Datasets	Chameleon	Squirrel	Actor	Texas	Cornell	Cora	Citeseer	Pubmed
$ \mathcal{V} $	2,277	5,201	7,600	183	183	2,708	3,327	19,717
ChebNet	59.51 $\pm$ 1.25	40.81 $\pm$ 0.42	37.42 $\pm$ 0.58	86.28 $\pm$ 2.62	83.91 $\pm$ 2.17	87.32 $\pm$ 0.92	79.33 $\pm$ 0.57	87.82 $\pm$ 0.24
ARMA	60.21 $\pm$ 1.00	36.27 $\pm$ 0.62	37.67 $\pm$ 0.54	83.97 $\pm$ 3.77	85.62 $\pm$ 2.13	87.13 $\pm$ 0.80	80.04 $\pm$ 0.55	86.93 $\pm$ 0.24
APPNP	52.15 $\pm$ 1.79	35.71 $\pm$ 0.78	39.76 $\pm$ 0.49	90.64 $\pm$ 1.70	91.52 $\pm$ 1.81	88.16 $\pm$ 0.74	80.47 $\pm$ 0.73	88.13 $\pm$ 0.33
GPRGNN	67.49 $\pm$ 1.38	50.43 $\pm$ 1.89	39.91 $\pm$ 0.62	92.91 $\pm$ 1.32	91.57 $\pm$ 1.96	88.54 $\pm$ 0.67	80.13 $\pm$ 0.84	88.46 $\pm$ 0.31
BernNet	68.53 $\pm$ 1.68	51.39 $\pm$ 0.92	41.71 $\pm$ 1.12	92.62 $\pm$ 1.37	92.13 $\pm$ 1.64	88.51 $\pm$ 0.92	80.08 $\pm$ 0.75	88.51 $\pm$ 0.39
ChebNetll	<b>71.37<math>\pm</math>1.01</b>	<b>57.72<math>\pm</math>0.59</b>	<b>41.75<math>\pm</math>1.07</b>	<b>93.28<math>\pm</math>1.47</b>	<b>92.30<math>\pm</math>1.48</b>	<b>88.71<math>\pm</math>0.93</b>	<b>80.53<math>\pm</math>0.79</b>	<b>88.93<math>\pm</math>0.29</b>
ClenshawGCN	<b>69.44<math>\pm</math>0.92</b>	<b>62.14<math>\pm</math>0.70</b>	<b>42.08<math>\pm</math>0.86</b>	<b>93.36<math>\pm</math>0.99</b>	<b>92.46<math>\pm</math>1.64</b>	<b>88.90<math>\pm</math>0.59</b>	<b>80.34<math>\pm</math>0.57</b>	<b>91.99<math>\pm</math>0.17</b>

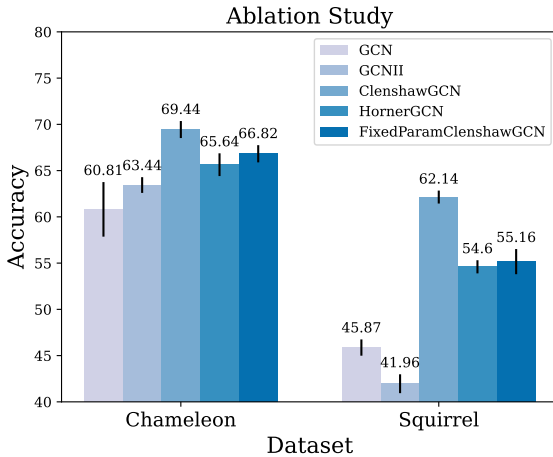


**Figure 2: Results of the ablation study. HornerGCN and FixedParamClenshawGCN are weakened versions of ClenshawGCN. HornerGCN is only equipped with adaptive initial residue, and FixedParamClenshawGCN is only equipped with negative second-order residue. The performance of these two ablation models are worse than a complete ClenshawGCN but outperform GCN and GCNII.**

*Ablation Model: FixedParamClenshawGCN.* In the FixedParamClenshawGCN model, we verify the contribution of *adaptive* initial residue by fixing  $\vec{\alpha} = [\hat{\alpha}_0, \hat{\alpha}_1, \dots, \hat{\alpha}_K]$  with

$$\hat{\alpha}_\ell = \alpha(1 - \alpha)^{K-\ell}, \quad \hat{\alpha}_0 = (1 - \alpha)^K$$

following APPNP [19], where  $\alpha \in [0, 1]$  is a hyperparameter. The corresponding polynomial filter of FixedParamClenshawGCN is:

$$h_{Fix}(\mu) = \sum_{\ell=0}^K \hat{\alpha}_{K-\ell} U_\ell(\mu).$$

*Analysis.* We compare the performance of HornerGCN and FixedParamClenshawGCN with GCN, GCNII and ClenshawGCN on two median-sized datasets: Chameleon and Squirrel. As shown in Figure 2, either removing the negative second-order residue or fixing the initial residue causes an obvious drop in Test Accuracy.

Noticeably, with only one residual module, HornerGCN and FixedParamClenshawGCN still outperform homophilic models such as GCNII. For HornerGCN, the reason is obvious: HornerGCN simulates any polynomial filter, which is favorable for heterophilic graphs. For FixedParamClenshawGCN, though the coefficients of  $U_\ell(\mu)$  are fixed, the contribution of each fixed level (*i.e.*  $\tilde{P}^\ell \mathbf{H}^*$ ) is no longer definitely to be *positive* as in GCNII since each chebyshev polynomial consists of terms with *alternating signs*, *e.g.*  $U_4(\tilde{P}) = 16\tilde{P}^4 - 12\tilde{P}^2 + 1$ , which breaks the underlying homophily assumption.



## 5 CONCLUSION

In this paper, we propose ClenshawGCN, a GNN model equipped with a novel and neat residual connection module that is able to mimic a spectral polynomial filter. When generating node representations for the next layer (i.e.  $\mathbf{H}^{(\ell+1)}$ ), our model should only connect to the initial layer (i.e.  $\mathbf{H}^{(0)}$ ) *adaptively*, and to the second last layer (i.e.  $\mathbf{H}^{(\ell-1)}$ ) *negatively*. The construction of this residual connection inherently uses Clenshaw Summation Algorithm, a numerical evaluation algorithm for calculating weighted sums of Chebyshev basis. We prove that our model implicitly simulates *any* polynomial filter based on the *second-kind Chebyshev basis* entangle with non-linear layers, bringing it at least comparable expressive power with state-of-art polynomial spectral GNNs. Experiments demonstrate our model's superiority either compared with other spatial models with residual connections or with spectral models.

For future work, a promising direction is to further investigate the mechanism and potential of such spectrally-inspired models entangled with non-linearity, which seems be able to incorporate the strengths of both sides.

## REFERENCES

- [1] Sami Abu-El-Hajja, Bryan Perozzi, Amol Kapoor, Nazanin Alipourfard, Kristina Lerman, Hrayr Harutyunyan, Greg Ver Steeg, and Aram Galstyan. 2019. Mixhop: Higher-order graph convolutional architectures via sparsified neighborhood mixing. In *international conference on machine learning*. PMLR, 21–29.
- [2] Takuya Akiba, Shotaro Sano, Toshihiko Yanase, Takeru Ohta, and Masanori Koyama. 2019. Optuna: A next-generation hyperparameter optimization framework. In *Proceedings of the 25th ACM SIGKDD international conference on knowledge discovery & data mining*. 2623–2631.
- [3] Filippo Maria Bianchi, Daniele Grattarola, Lorenzo Livi, and Cesare Alippi. 2021. Graph neural networks with convolutional arma filters. *IEEE Transactions on Pattern Analysis and Machine Intelligence* (2021).
- [4] Peter J Burt and Edward H Adelson. 1987. The Laplacian pyramid as a compact image code. In *Readings in computer vision*. Elsevier, 671–679.
- [5] Ben Chamberlain, James Rowbottom, Maria I Gorinova, Michael Bronstein, Stefan Webb, and Emanuele Rossi. 2021. Grand: Graph neural diffusion. In *International Conference on Machine Learning*. PMLR, 1407–1418.
- [6] Ming Chen, Zhewei Wei, Zengfeng Huang, Bolin Ding, and Yaliang Li. 2020. Simple and deep graph convolutional networks. In *ICML*. PMLR, 1725–1735.
- [7] Eli Chien, Jianhao Peng, Pan Li, and Olga Milenkovic. 2021. Adaptive Universal Generalized PageRank Graph Neural Network. In *ICLR*.
- [8] Mark Craven, Andrew McCallum, Dan PiPasquo, Tom Mitchell, and Dayne Freitag. 1998. *Learning to extract symbolic knowledge from the World Wide Web*. Technical Report. Carnegie-mellon univ pittsburgh pa school of computer Science.
- [9] Michaël Defferrard, Xavier Bresson, and Pierre Vandergheynst. 2016. Convolutional Neural Networks on Graphs with Fast Localized Spectral Filtering. (6 2016). <http://arxiv.org/abs/1606.09375>
- [10] David K Duvenaud, Dougal Maclaurin, Jorge Iparraguirre, Rafael Bombarell, Timothy Hirzel, Alan Aspuru-Guzik, and Ryan P Adams. 2015. Convolutional networks on graphs for learning molecular fingerprints. *Advances in neural information processing systems* 28 (2015).
- [11] Wenqi Fan, Yao Ma, Qing Li, Yuan He, Eric Zhao, Jiliang Tang, and Dawei Yin. 2019. Graph neural networks for social recommendation. In *The world wide web conference*. 417–426.
- [12] Kaiming He, Xiangyu Zhang, Shaoqing Ren, and Jian Sun. 2016. Deep Residual Learning for Image Recognition. In *Proceedings of the IEEE Conference on Computer Vision and Pattern Recognition (CVPR)*.
- [13] Mingguo He, Zhewei Wei, Zengfeng Huang, and Hongteng Xu. 2021. BernNet: Learning Arbitrary Graph Spectral Filters via Bernstein Approximation. *Advances in Neural Information Processing Systems* 34 (6 2021), 14239–14251. <http://arxiv.org/abs/2106.10994>
- [14] Mingguo He, Zhewei Wei, and Ji-Rong Wen. 2022. Convolutional Neural Networks on Graphs with Chebyshev Approximation, Revisited. *arXiv preprint arXiv:2202.03580* (2022).
- [15] William George Horner. 1819. XXI. A new method of solving numerical equations of all orders, by continuous approximation. *Philosophical Transactions of the Royal Society of London* 109 (1819), 308–335.
- [16] Forrest Iandola, Matt Moskewicz, Sergey Karayev, Ross Girshick, Trevor Darrell, and Kurt Keutzer. 2014. Densenet: Implementing efficient convnet descriptor pyramids. *arXiv preprint arXiv:1404.1869* (2014).
- [17] Diederik P Kingma and Jimmy Ba. 2014. Adam: A method for stochastic optimization. *arXiv preprint arXiv:1412.6980* (2014).
- [18] Thomas N Kipf and Max Welling. 2017. Semi-supervised classification with graph convolutional networks. In *ICLR*.
- [19] Johannes Klicpera, Aleksandar Bojchevski, and Stephan Günnemann. 2019. Predict then propagate: Graph neural networks meet personalized pagerank. In *ICLR*.
- [20] Johannes Klicpera, Stefan Weissenberger, and Stephan Günnemann. 2019. Diffusion improves graph learning. *arXiv preprint arXiv:1911.05485* (2019).
- [21] Guohao Li, Matthias Müller, Ali Thabet, and Bernard Ghanem. 2019. DeepGCNs: Can GCNs Go as Deep as CNNs? (4 2019). <http://arxiv.org/abs/1904.03751>
- [22] Qimai Li, Zhichao Han, and Xiao-Ming Wu. 2018. Deeper insights into graph convolutional networks for semi-supervised learning. In *Thirty-Second AAAI conference on artificial intelligence*.
- [23] Derek Lim, Felix Hohne, Xiuyu Li, Sijia Linda Huang, Vaishnavi Gupta, Omkar Bhalerao, and Ser-Nam Lim. 2021. Large Scale Learning on Non-Homophilous Graphs: New Benchmarks and Strong Simple Methods. *Advances in Neural Information Processing Systems* 34 (10 2021), 20887–20902. <http://arxiv.org/abs/2110.14446>
- [24] Xiaorui Liu, Jiayuan Ding, Wei Jin, Han Xu, Yao Ma, Zitao Liu, and Jiliang Tang. 2021. Graph Neural Networks with Adaptive Residual. *NIPS* (2021). <https://github.com/lxiaorui/AirGNN>.
- [25] Sitao Luan, Chenqing Hua, Qincheng Lu, Jiaqi Zhu, Mingde Zhao, Shuyuan Zhang, Xiao-Wen Chang, and Doina Precup. 2021. Is Heterophily A Real Nightmare For Graph Neural Networks To Do Node Classification? (9 2021). <http://arxiv.org/abs/2109.05641>
- [26] Miller McPherson, Lynn Smith-Lovin, and James M Cook. 2001. Birds of a feather: Homophily in social networks. *Annual review of sociology* (2001), 415–444.
- [27] Sunil K Narang, Akshay Gadde, and Antonio Ortega. 2013. Signal processing techniques for interpolation in graph structured data. In *2013 IEEE International Conference on Acoustics, Speech and Signal Processing*. IEEE, 5445–5449.
- [28] Sylvain Paris, Samuel W Hasinoff, and Jan Kautz. 2011. Local laplacian filters: edge-aware image processing with a laplacian pyramid. *ACM Trans. Graph.* 30, 4 (2011), 68.
- [29] Hongbin Pei, Bingzhe Wei, Kevin Chen-Chuan Chang, Yu Lei, and Bo Yang. 2020. Geom-GCN: Geometric Graph Convolutional Networks. In *ICLR*.
- [30] Bryan Perozzi and Leman Akoglu. 2018. Discovering communities and anomalies in attributed graphs: Interactive visual exploration and summarization. *ACM Transactions on Knowledge Discovery from Data* (TKDD) 12, 2 (2018), 1–40.
- [31] Yu Rong, Wenbing Huang, Tingyang Xu, and Junzhou Huang. 2020. DropEdge: Towards Deep Graph Convolutional Networks on Node Classification. In *ICLR*.
- [32] Victor Garcia Satorras, Emiel Hoogeboom, and Max Welling. 2021. E (n) equivariant graph neural networks. In *International conference on machine learning*. PMLR, 9323–9332.
- [33] Michael Sejr Schlichtkrull, Nicola De Cao, and Ivan Titov. 2020. Interpreting graph neural networks for nlp with differentiable edge masking. *arXiv preprint arXiv:2010.00577* (2020).
- [34] Prithviraj Sen, Galileo Namata, Mustafa Bilgic, Lise Getoor, Brian Galligher, and Tina Eliassi-Rad. 2008. Collective classification in network data. *AI magazine* 29, 3 (2008), 93–93.
- [35] David I Shuman, Benjamin Ricaud, and Pierre Vandergheynst. 2013. Vertex-Frequency Analysis on Graphs. (7 2013). <http://arxiv.org/abs/1307.5708>
- [36] Ilya Sutskever, James Martens, George Dahl, and Geoffrey Hinton. 2013. On the importance of initialization and momentum in deep learning. In *International conference on machine learning*. PMLR, 1139–1147.
- [37] Jie Tang, Jimeng Sun, Chi Wang, and Zi Yang. 2009. Social influence analysis in large-scale networks. In *Proceedings of the 15th ACM SIGKDD international conference on Knowledge discovery and data mining*. 807–816.
- [38] Guangtao Wang, Rex Ying, Jing Huang, and Jure Leskovec. 2019. Improving graph attention networks with large margin-based constraints. *arXiv preprint arXiv:1910.11945* (2019).
- [39] Xiuyan Wang and Muhan Zhang. 2022. How Powerful are Spectral Graph Neural Networks. (5 2022). <http://arxiv.org/abs/2205.11172>
- [40] Lingfei Wu, Yu Chen, Kai Shen, Xiaojie Guo, Hanning Gao, Shucheng Li, Jian Pei, and Bo Long. 2021. Graph neural networks for natural language processing: A survey. *arXiv preprint arXiv:2106.06090* (2021).
- [41] Shiwu Wu, Fei Sun, Wentao Zhang, Xu Xie, and Bin Cui. 2020. Graph neural networks in recommender systems: a survey. *ACM Computing Surveys (CSUR)* (2020).
- [42] Keyulu Xu, Chengtao Li, Yonglong Tian, Tomohiro Sonobe, Ken-ichi Kawarabayashi, and Stefanie Jegelka. 2018. Representation Learning on Graphs with Jumping Knowledge Networks. In *ICML*.
- [43] Liang Yang, Weihang Peng, Wenmiao Zhou, Bingxin Niu, Junhua Gu, Chuan Wang, Yuanfang Guo, Xiaochun Cao, and Dongxiao He. 2022. Difference Residual Graph Neural Networks. *ACMMM22* (2022). <https://doi.org/10.1145/3503161>.

- 3548111
- [44] Zhilin Yang, William Cohen, and Ruslan Salakhudinov. 2016. Revisiting semi-supervised learning with graph embeddings. In International conference on machine learning. PMLR, 40–48.
- [45] Wentao Zhang, Zeang Sheng, Ziqi Yin, Yuezhian Jiang, Yikuan Xia, Jun Gao, Zhi Yang, and Bin Cui. 2022. Model Degradation Hinders Deep Graph Neural Networks. Proceedings of the 28th ACM SIGKDD Conference on Knowledge Discovery and Data Mining, 2493–2503. <https://doi.org/10.1145/3534678.3539374>
- [46] Jialin Zhao, Yuxiao Dong, Ming Ding, Evgeny Kharlamov, and Jie Tang. 2021. Adaptive Diffusion in Graph Neural Networks. Advances in Neural Information Processing Systems 34 (2021), 23321–23333.
- [47] Xin Zheng, Yixin Liu, Shirui Pan, Miao Zhang, Di Jin, and Philip S Yu. 2022. Graph neural networks for graphs with heterophily: A survey. arXiv preprint arXiv:2202.07082 (2022).
- [48] Jiong Zhu, Yujun Yan, Lingxiao Zhao, Mark Heimann, Leman Akoglu, and Danai Koutra. 2020. Beyond homophily in graph neural networks: Current limitations and effective designs. Advances in Neural Information Processing Systems 33 (2020), 7793–7804.